Sohn and Gwak *EURASIP Journal on Wireless Communications and Networking* (2016) 2016:37
DOI 10.1186/s13638-016-0538-z

EURASIP Journal on Wireless Communications and Networking
a SpringerOpen Journal

RESEARCH Open Access

Single-RF MIMO-OFDM system with beam switching antenna

Illsoo Sohn[1] and Donghyuk Gwak[2*]

Abstract

In this paper, we investigate the replica interference problem of a multiple input multiple output (MIMO) receiver with a beam switching antenna (BSA) within the orthogonal frequency division multiplexing (OFDM) framework. Our frequency-domain analysis has revealed the following important findings: (i) without co-existing system, replica interference in the system can be completely avoided as long as the beam pattern switching rate of the BSA receiver is an integer multiple of the product of the OFDM sampling rate and the number of receiving beam patterns and (ii) with co-existing systems, replica interference cannot always be avoided because co-existing systems may induce replicas in the operating frequency bands of the system. We present a replica interference criterion that depends on the co-existing status and users beam switching capabilities. Based on our findings, we propose various replica interference avoidance (RINA) strategies for different co-existing and cooperating network scenarios. In addition, the overall network operation principles of the proposed RINA strategy are presented. Simulation results verify that the proposed MIMO-OFDM system with a BSA successfully provides both MIMO and OFDM benefits, thereby resolving replica interference issues.

Keywords: Multiple input multiple output, Beam switching antenna, Single-RF MIMO receiver, Spread spectrum, Co-channel interference

1 Introduction

In the last decade, multiple input multiple output (MIMO) techniques have been rigorously developed to dramatically increase wireless throughput and reliability [1–6]. Most of the recent wireless standards were initially designed in a MIMO framework. For example, the most popular recent commercial wireless systems such as 3GPP-LTE/A [7–9] and IEEE802.11n/11ac [10, 11] adopt MIMO techniques as a key feature. In the ongoing 5G wireless system standardization, various MIMO evolutions are under discussion to maximize MIMO benefits, which include the use of mmWAVE [12–15] and 3D-MIMO [16, 17]. In line with the technical evolution of MIMO, the number of antenna elements has been significantly increasing: four in LTE Rel-8 and eight in LTE Rel-10; a two-digit number is expected for 5G systems.

However, advanced wireless systems are facing two implementation problems at the cost of increased MIMO benefits. First, the increased number of antenna elements requires an increased number of RF front-ends, which directly increases implementation complexity, i.e., costs and power consumption. Second, the physical dimensions of MIMO devices will inevitably increase because the minimum spacing between antenna elements must be guaranteed for MIMO techniques. Typically, these problems can be managed at the base station (BS). However, they can become critical, especially in mobile devices. A strong demand for low cost, low power consumption, and small physical dimension devices has been limiting the number of implementable antennas in mobile devices. As an effort to resolve these problems, beam-steerable antenna concept has been studied in [18–24]. Beam-steerable antennas can be implemented using only a single active antenna with a single-RF front-end, reducing the required physical dimensions and costs. Beam-steering antennas operate equivalently with conventional linear array antennas by dynamically steering beam patterns using parasitic antenna elements. The performance of beam-steerable antennas at a single-RF MIMO receiver has been analyzed in [25]. In [26, 27], a beam switching antenna (BSA) has been proposed for use in a single-RF

*Correspondence: gwakdh@etri.re.kr
[2]Communications and Internet Research Lab., ETRI, 305-700 Daejeon, Korea
Full list of author information is available at the end of the article

MIMO receiver as a simplified form of beam-steerable antenna. In [28, 29], BSAs are utilized at user devices and improve multi-user system throughput by exploiting pattern diversity. Figure 1 provides a conceptual diagram of a BSA. A BSA predetermines discrete beam patterns and rapidly switches between them using PIN diodes, which makes it very useful for practical implementations. In particular, recent advances in PIN diodes enable very fast switching speed up to 1–100 ns [30, 31], which make BSAs more attractive. Thus, we focus on the single-RF MIMO receiver with a BSA in this work.

It has been first revealed in [25] that the beam-steering nature of a single-RF MIMO receiver induces replicas in the frequency domain. The induced replicas may interfere with the desired signals, which is the major drawback of this type of antenna. A more detailed analysis of the impacts of replicas in a single-RF MIMO receiver with a BSA is presented in [27]. Several restrictions on beam pattern switching rates to avoid replica interference have been presented. However, all of the aforementioned works in this field assume an idealized system model, e.g., a single-carrier system and no co-existing systems. For practical applications of a single-RF MIMO receiver with a BSA, a more realistic system model is essential. In this paper, we investigate a single-RF MIMO receiver with a BSA assuming a practical wireless system. We consider a multi-carrier system, specifically, an orthogonal frequency division multiplexing (OFDM) system, with co-existing systems in neighboring frequency bands. Replica interference scenarios in this case become very complicated, and a sophisticated control scheme is required to avoid them. We propose a practical single-RF MIMO-OFDM system with a BSA that resolves replica interference problem. Compared to two most closely related works in [25, 27], this paper includes the following differential work and novelty. In contrast to continuously rotating antennas in [25], we investigate beam switching antennas, which improves implementation feasibility with the help of rapid advances in electrical switching devices, e.g., PIN diodes. In [27], only single-carrier system model is considered for the simplicity of analysis while this paper extends the system model to capture multi-carrier and co-existing system scenarios. Thus, this paper provides more practical results for real-world communication environments.

The main contributions of this paper can be summarized as follows.

- **BSA for multi-carrier systems:** We generalize a single-RF MIMO receiver with a BSA within an OFDM framework. We have investigated the beam pattern switching rate of the BSA required to avoid replica interference. Our frequency-domain analysis has revealed that replica interference can be completely avoided if the beam pattern switching rate of the BSA receiver is an integer multiple of the product of the OFDM sampling rate and the number of receiving beam patterns. To the best of our knowledge, this has never been studied in the literature.

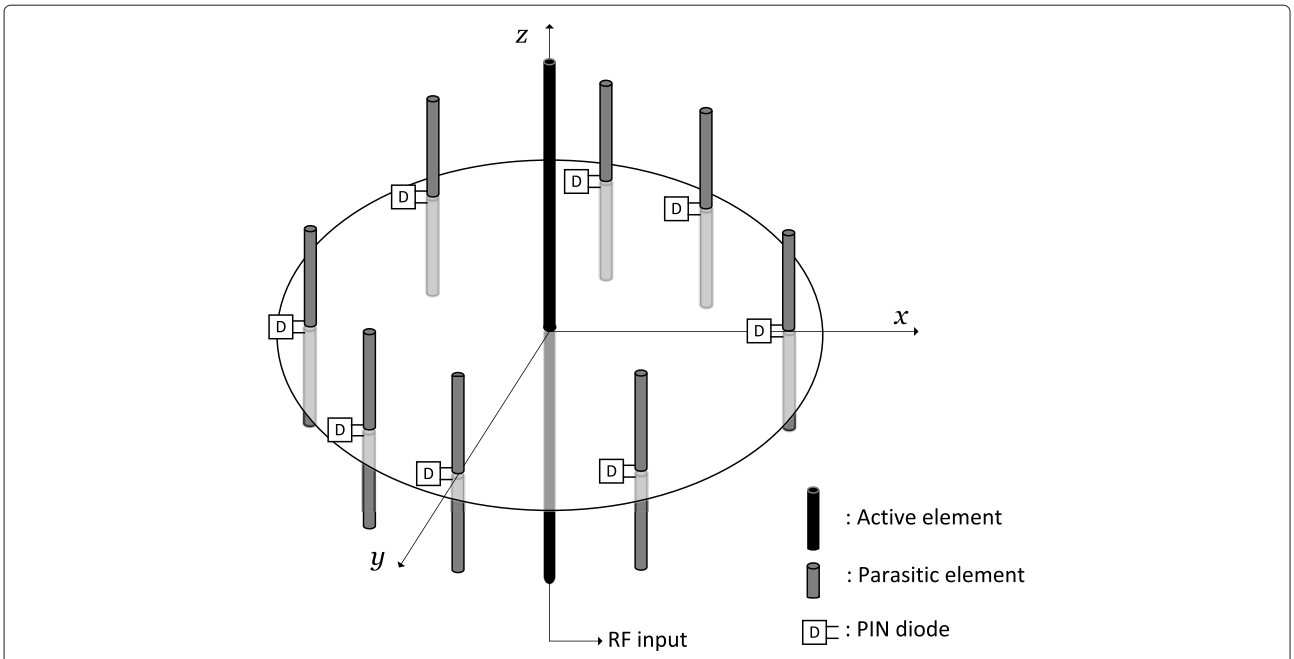

Fig. 1 Beam switching antenna with eight parasitic elements

- **Co-existence strategies:** We consider the practical case in which there are co-existing systems in the neighboring frequency bands. We have derived mathematical conditions under which co-existing systems interfere with each other by inducing replicas. Possible co-existing and cooperating scenarios are classified. Then, we propose the most appropriate replica interference avoidance (RINA) strategy for each case.
- **Overall network operations:** Based on the proposed co-existence strategies, we present the overall network operation principles for a single-RF MIMO-OFDM system with a BSA. The distinguishing feature of the proposed system is that the beam switching capabilities of user devices are initially reported to the BS. The scheduler at the BS uses this information for user and subcarrier allocation. Then, the scheduling information (including selected users, subcarrier, and the corresponding beam pattern switching rates) is broadcasted.

The remainder of this paper is organized as follows. Our system model is described in Section 2. Frequency-domain analysis of replica interference in single-RF MIMO-OFDM systems is presented in Section 3. In Section 4, various strategies for replica interference avoidance are proposed and compared. The overall network operation of the proposed single-RF MIMO-OFDM system with a BSA is explained in Section 5. Simulation results are presented in Section 6. Finally, conclusions are drawn in Section 7.

Notation. Upper case boldface letters and lower case boldface letters are used for matrices and vectors, respectively. Matrix operators $(\cdot)^T$, $(\cdot)^H$, and $(\cdot)^{-1}$ respectively denote transpose, conjugate transpose, and inverse operations. $\mathbb{F}\{\cdot\}$ denotes the Fourier transform, $\delta(\cdot)$ denotes the Dirac delta function, operation $*$ denotes the convolution of signals, and $\mathbf{I}_N$ denotes an N-by-N identity matrix. The following is a summary of the mathematical notations that will be frequently used in this paper:

- N_{T}: total number of transmitting beam patterns
- M_{R}: total number of switching beam patterns of user
- N_{U}: total number of users
- N_{S}: total number of OFDM subcarriers
- N_{B}: total number of co-existing systems
- T_{OFDM}: OFDM symbol duration
- f_{S}: OFDM sampling frequency
- T_{S}: OFDM sample duration
- Ω: oversampling factor of a BSA
- f_{SW}: beam pattern switching rate of a BSA
- n: transmitting beam patter index, $m = 1, 2, \ldots, N_{\mathrm{T}}$
- m: receiving beam pattern index, $n = 1, 2, \ldots, M_{\mathrm{R}}$
- u: user index, $u = 1, 2, \ldots, N_{\mathrm{U}}$
- k: subcarrier index, $k = 1, 2, \ldots, N_{\mathrm{S}}$
- $\mathcal{B}$: set of co-existing system subbands
- $\mathcal{U}$: set of all users
- $\mathcal{S}$: set of selected users
- Φ: set of all subcarriers
- Ψ: set of selected subcarriers
- $\mathcal{W}$: set of selected beam pattern switching rates

2 System model

Figure 2 depicts the system model in this work. We consider a downlink OFDM system with one BS and N_{U} users. The BS has multiple transmit antennas in a conventional linear array form, whereas each user device utilizes a BSA. The BSA at each user consists of one active antenna connected to an RF front-end and M_{R} parasitic elements. By controlling these parasitic elements with PIN diodes, the BSA generates M_{R} beam patterns and switches between them. The OFDM symbol duration is T_{OFDM}, the number of OFDM subcarriers is N_{S}, OFDM sampling rate is f_{S}, and OFDM sample duration is T_{S}. For every OFDM sampling instances, the BSA sequentially switches all M_{R} beam patterns, collecting M_{R} different versions of the received signal. For simplicity, we assume that the allocated time for each beam pattern is the same. Thus, the beam pattern switching rate of the BSA should be a multiple of the OFDM sampling rate and the number of receiving beam patterns as $f_{\mathrm{SW}} = \Omega M_{\mathrm{R}} f_{\mathrm{S}}$, where Ω denotes an oversampling factor. For example, integer values of $\Omega(\geq 1)$ indicates the number of times that the BSA repeats sweeping the M_{R} beam patterns for each OFDM sample. This number is closely related to the processing capability of the user device. We consider different beam pattern switching capabilities for different on users.

We consider a beamspace-domain MIMO channel model [27, 32] that represents a MIMO channel matrix with channel gains between the transmitting beam patterns and receiving beam patterns. The channel matrix between the BS and user u is $\mathbf{H}_u$, where the element in the mth row and the nth column denotes the channel gain between the nth transmitting beam pattern at the BS and the mth receiving beam pattern at user u. The received signal at the BSA input of user u is

$$\mathbf{y}_u = \sqrt{\frac{\rho}{N_{\mathrm{T}}}}\mathbf{H}_u\mathbf{x}_u + \mathbf{v}_u, \tag{1}$$

where $\mathbf{x}_u$ is an $N_{\mathrm{T}} \times 1$ vector representing the transmitting signals, and satisfying $\mathbb{E}\left[\mathbf{x}_u\mathbf{x}_u^H\right] = \mathbf{I}_{N_{\mathrm{T}}}$, $\mathbf{v}_u$ is an $M_{\mathrm{R}} \times 1$ noise vector with $\mathbb{E}\left[\mathbf{v}_u\mathbf{v}_u^H\right] = \mathbf{I}_{M_{\mathrm{R}}}$, $\mathbf{H}_u$ is an $M_{\mathrm{R}} \times N_{\mathrm{T}}$ complex channel gain matrix, $\mathbf{y}_u = \left[y_{u,1}, \ldots, y_{u,m}, \ldots, y_{u,M_{\mathrm{R}}}\right]^T$ is an $M_{\mathrm{R}} \times 1$ vector representing the received signals, where the mth element, $y_{u,m}$ denotes the received signal

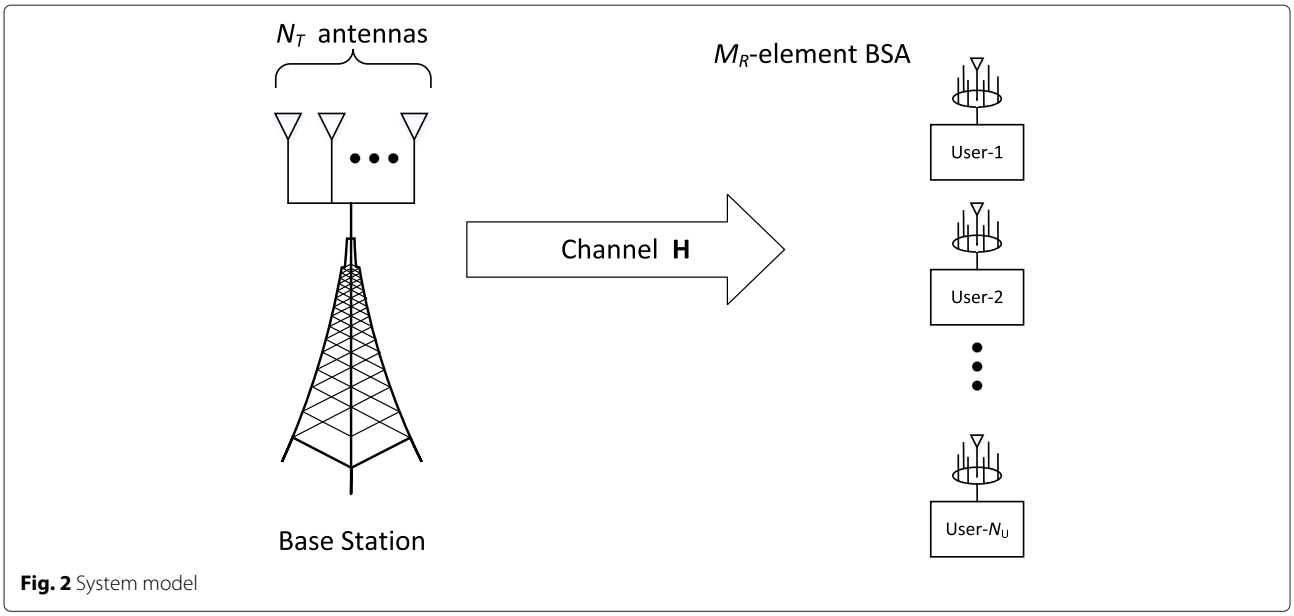

Fig. 2 System model

via the mth receiving beam pattern. The effective received signal of user u at the BSA output is

$$r_u(t) = \sum_{m=1}^{M_R} \sum_{i=-\infty}^{\infty} \Pi\left(\frac{t-(m-1)\frac{T_S}{\Omega M_R} - i\frac{T_S}{\Omega}}{\frac{T_S}{\Omega M_R}} \right) y_{u,m}(t), \tag{2}$$

where $\Pi(t)$ can be defined as

$$\Pi(t) = \begin{cases} 1, & \text{if } -\frac{1}{2} < t \le \frac{1}{2} \\ 0, & \text{otherwise.} \end{cases} \tag{3}$$

Note that the effective received signal at the BSA output is in the time-multiplexed form of the BSA input signals $\mathbf{y}_u$ as illustrated in Fig. 3.

In practical wireless service scenarios, one or more systems may co-exist in the neighboring frequency bands. The operating frequency bands of the co-existing systems are set to be mutually exclusive, assuming there is no out-of-band interference between them. The co-existing systems can be secondary carriers of the same network operator, carriers of other network operators, or completely different radio access systems, e.g., non-OFDM systems. Cooperating scenarios may vary depending on co-existing status, which will be specified in Section 4.

3 Replica interference in a single-RF MIMO-OFDM system

In this section, we investigate replica interference in a single-RF MIMO-OFDM system with a BSA. First, we preform frequency-domain analysis. Then, we reveal the required beam pattern switching rate to avoid replica interference, both with and without co-existing systems.

3.1 Frequency-domain analysis

The beam switching nature of a BSA receiver inevitably induces replicas in the frequency spectrum [25, 27]. The frequency-domain analysis that follows aims to determine the positions of the induced replicas and the extent to which the replicas interfere with the desired signal. The analysis of replicas is very important to the implementation of practical wireless systems. Before we compute the Fourier transform, the effective received signal in (2) is rewritten as

$$r(t) = \sum_{m=1}^{M_R} \left[\left\{ \delta\left(t-(m-1)\frac{T_S}{\Omega M_R} \right) * \left(\sum_{i=-\infty}^{\infty} \delta\left(t - i\frac{T_S}{\Omega} \right) \right) * \Pi\left(\frac{t}{T_S/\Omega M_R} \right) \right\} y_m(t) \right]. \tag{4}$$

Then, we compute the Fourier transform of the signal $R(f) = \mathbb{F}\{r(t)\}$ as

$$R(f) = \sum_{m=1}^{M_R} \left[\left\{ \underbrace{\mathbb{F}\left\{ \delta\left(t-(m-1)\frac{T_S}{\Omega M_R} \right) \right\}}_{(a)} \underbrace{\mathbb{F}\left\{ \left(\sum_{i=-\infty}^{\infty} \delta\left(t - i\frac{T_S}{\Omega} \right) \right) \right\}}_{(b)} \underbrace{\mathbb{F}\left\{ \Pi\left(\frac{t}{T_S/\Omega M_R} \right) \right\}}_{(c)} \right\} * Y_m(f) \right]. \tag{5}$$

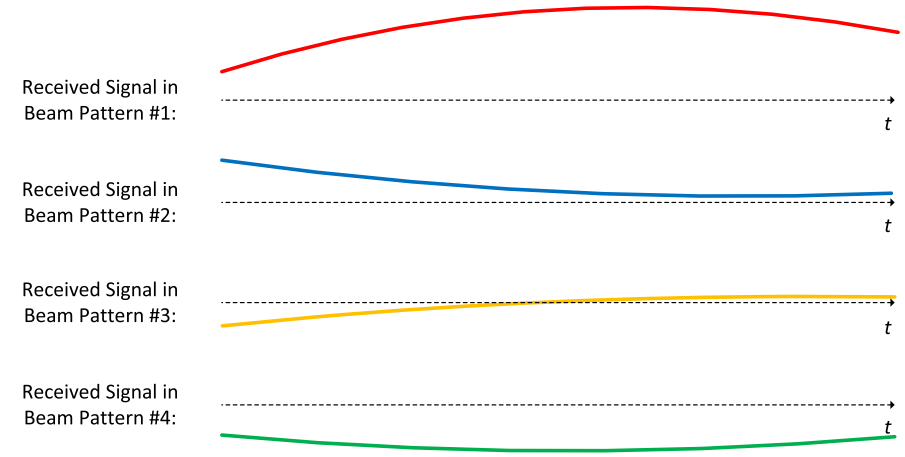

(a) Received signals at the BSA input

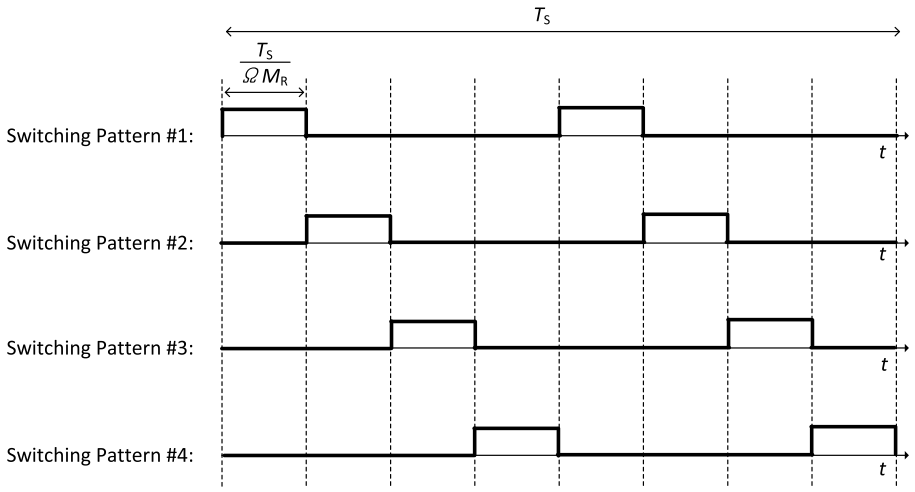

(b) Beam switching patterns

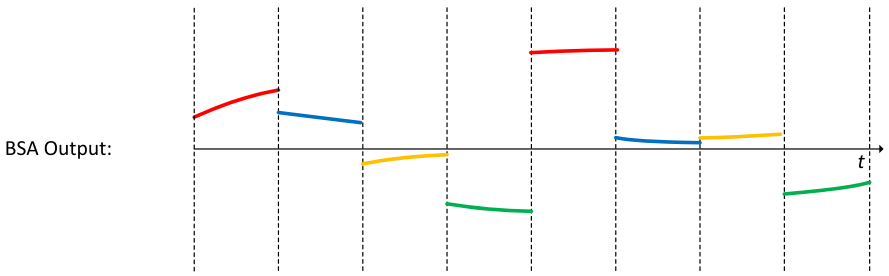

(c) Effective received signal at the BSA output

Fig. 3 Example of received signal at the BSA with $M_R = 4$ and $\Omega = 2$

For further derivations of Fourier transforms, (*a*) uses the time-shift property as

$$\mathbb{F}\left\{\delta\left(t-(m-1)\frac{T_S}{\Omega M_R}\right)\right\}=e^{-j2\pi\frac{(m-1)T_S}{\Omega M_R}f}, \tag{6}$$

(*b*) uses the fact that the Fourier transform of an impulse train is also an impulse train as

$$\mathbb{F}\left\{\left(\sum_{i=-\infty}^{\infty}\delta\left(t-i\frac{T_S}{\Omega}\right)\right)\right\}=\frac{\Omega}{T_S}\sum_{l=-\infty}^{\infty}\delta\left(f-l\frac{\Omega}{T_S}\right), \tag{7}$$

and (*c*) uses the fact that the Fourier transform of a rectangular pulse becomes a sinc(·) function and applies the time-scaling property as

$$\mathbb{F}\left\{\Pi\left(\frac{t}{T_S/\Omega M_R}\right)\right\}=\frac{T_S}{\Omega M_R}\mathrm{sinc}\left(\frac{T_S}{\Omega M_R}f\right) \tag{8}$$

Putting (6), (7), and (8) into (5) gives

$$\begin{aligned}R(f)&=\sum_{m=1}^{M_R}\left[\left\{e^{-j2\pi\frac{(m-1)T_S}{\Omega M_R}f}\left(\sum_{l=-\infty}^{\infty}\delta\left(f-l\frac{\Omega}{T_S}\right)\right)\right.\right.\\&\quad\left.\left.\times\frac{1}{M_R}\mathrm{sinc}\left(\frac{T_S}{\Omega M_R}f\right)\right\}*Y_m(f)\right]\\&=\sum_{m=1}^{M_R}\left[\left\{\sum_{l=-\infty}^{\infty}e^{-j2\pi\frac{(m-1)}{M_R}l}\frac{1}{M_R}\mathrm{sinc}\left(\frac{l}{M_R}\right)\right.\right.\\&\quad\left.\left.\times\delta\left(f-l\frac{\Omega}{T_S}\right)\right\}*Y_m(f)\right]\\&=\sum_{m=1}^{M_R}\left[\left\{\sum_{l=-\infty}^{\infty}\underbrace{e^{-j2\pi\frac{(m-1)}{M_R}l}}_{(a)}\underbrace{\frac{1}{M_R}\mathrm{sinc}\left(\frac{l}{M_R}\right)}_{(b)}\right.\right.\\&\quad\left.\left.\times\underbrace{\delta\left(f-\Omega f_S l\right)}_{(c)}\right\}*Y_m(f)\right].\end{aligned} \tag{9}$$

The frequency-domain analysis results can be interpreted as follows. From (*c*), the received signal at the BSA input $Y_m(f)$ induces an infinite number of replicas at frequencies of $f=\Omega f_S l$, where l is an integer number from $-\infty$ to ∞. Hereafter, we refer to the frequency specified by l as the lth subband. The replicas at different subbands are not in an equivalent form. The phase shift of the replica in the lth subband is specified by (*a*). The phase shifting pattern is repeated every M_R consecutive subbands. On the other hand, (*b*) specifies the amplitude of the replica in the lth subband. Considering $l=0$ as the center frequency, the replicas vanish at every M_R subbands. The amplitude of the replicas gradually decreases as we move away from the center. The main lobe contains $2M_R-1$ subbands while the side lobes contain only M_R-1 subbands. In addition, the replicas corresponding to different received signals from different beam patterns are overlaid at the same subband positions. Figure 4 illustrates the power spectral density of the BSA output.

3.2 Self-replica interference

Using frequency-domain analysis, we have revealed the exact positions of the induced replicas. Here, we assume that there are no co-existing systems. According to (9), each subband is composed of a summation of the received signals at different receiving beam patterns. Since (a) and (b) simply change phases and amplitudes, the bandwidth of each subband remains the same with the transmitted signal, i.e., f_S. From (9), the spacing between the adjacent replicas is Ωf_S. Accordingly, the required condition under which the replicas do not overlap and interfere with each other is $\Omega f_S \geq f_S$. Note that Ω is the oversampling factor of a BSA and is an integer greater than or equal to one ($\Omega \geq 1$). This analysis confirms that the required condition above is always satisfied for this definition of Ω.

Remark. In a single-RF MIMO-OFDM receiver with a BSA, replica interference can be completely avoided if the beam pattern switching rate of the BSA receiver is an integer multiple of the product of the OFDM sampling rate and the number of receiving beam patterns. In other words, there will be no performance degradation due to self-replica interference.

3.3 Replica interference from co-existing systems

If co-existing systems are present, replica interference scenarios become very complicated. For simplicity, the co-existing systems are assumed to have the same system bandwidth and are located at one of the subbands. We denote the subband index occupied by the reference system by b_0, and the set of neighboring subbands in which co-existing systems are located by $\mathcal{B}=\{1,2,\cdots,N_B\}$. We know from the analysis above that the replicas of a system arise in every Ωth subband starting from the center subband occupied by the system itself. Thus, the criterion that the co-existing systems do not induce their replicas in the subbands of the reference system can be written as

$$\mathrm{mod}(b_0,\Omega)\neq\mathrm{mod}(b,\Omega), \quad \text{for } b\in\mathcal{B}. \tag{10}$$

The amount of replica interference experienced by the reference system varies depending on the total number of co-existing systems and their relative distributions in the frequency domain. In the next section, we will develop sophisticated strategies for replica interference avoidance. These strategies are designed for use in different co-existing and cooperating scenarios.

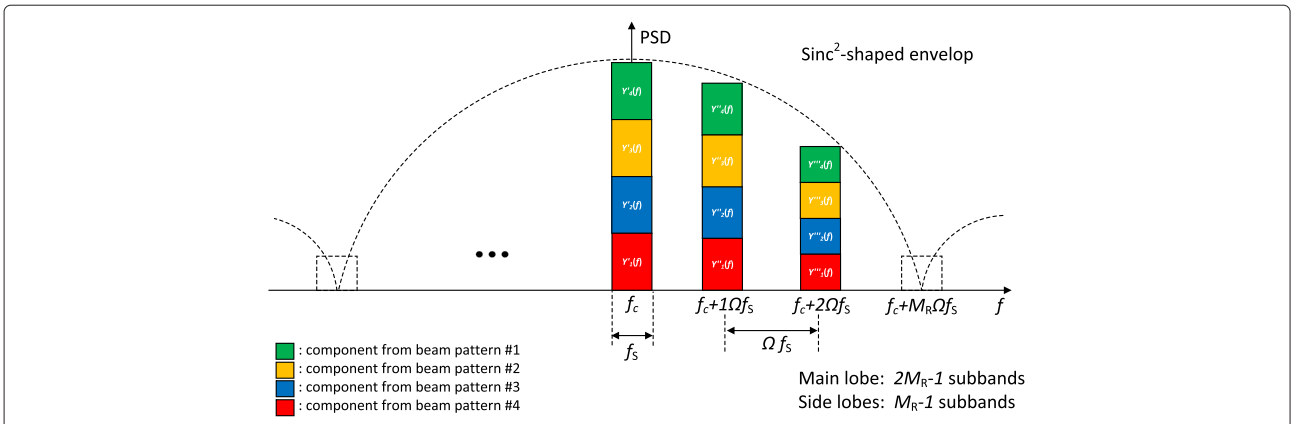

Fig. 4 Illustration of power spectral density of a BSA output

3.4 Sum capacity with the presence of replica interference

In this subsection, we derive the capacity of the system considering the presence of replica interference. First, we denote $W_l(f)$ as the replica of the system that appears in the lth subband ($l = -\infty, \ldots, 0, \ldots, \infty$). As observed from (9), the replicas are repeated in every M_R subbands with scaled amplitudes. Hence, M_R consecutive subbands contain independent information regarding the transmitted signals. Thus, we select the M_R centermost replicas to recover the transmitted data, because they are located in the main lobe of the sinc function, and therefore, have the highest powers. Let $\mathbf{W}(f) = \left[W_{l_{\min}}(f), \ldots, W_{l_{\max}}(f)\right]^T$ denotes the vector of the selected subbands, where

$$(l_{\min}, l_{\max}) = \begin{cases} \left(-\frac{M_R-1}{2}, \frac{M_R-1}{2}\right), & \text{if } M_R \text{ is odd,} \\ \left(-\frac{M_R}{2}+1, \frac{M_R}{2}\right), & \text{if } M_R \text{ is even.} \end{cases} \tag{11}$$

Let $\mathbf{G}$ denotes a transfer matrix between $\mathbf{W}(f)$ and $\mathbf{Y}(f) = \left[Y_1(f), Y_2(f), \ldots, Y_{M_R}(f)\right]^T$ as

$$\mathbf{W}(f) = \mathbf{G}\mathbf{Y}(f), \tag{12}$$

where

$$\mathbf{G} = \frac{1}{M_R}\Lambda\Gamma, \tag{13}$$

$$\Lambda = \begin{bmatrix} \mathrm{sinc}\left(\frac{l_{\min}}{M_R}\right) & \cdots & 0 \\ \vdots & \ddots & \vdots \\ 0 & \cdots & \mathrm{sinc}\left(\frac{l_{\max}}{M_R}\right) \end{bmatrix}, \tag{14}$$

$$\Gamma = \begin{bmatrix} 1 & \gamma^{l_{\min}} & \cdots & \gamma^{(M_R-1)l_{\min}} \\ \vdots & \vdots & \vdots & \vdots \\ 1 & 1 & \cdots & 1 \\ \vdots & \vdots & \vdots & \vdots \\ 1 & \gamma^{l_{\max}} & \cdots & \gamma^{(M_R-1)l_{\max}} \end{bmatrix}, \tag{15}$$

$$\gamma = e^{-j2\pi\frac{1}{M_R}}. \tag{16}$$

Hence, the input vector of the user u for MIMO processing is

$$\mathbf{W}_u = \sqrt{\frac{\rho}{N_T}}\mathbf{G}\mathbf{H}_u\mathbf{X}_u + \mathbf{V}'_u, \tag{17}$$

where $\mathbf{V}'_u$ is defined as

$$\mathbf{V}'_u = \begin{bmatrix} \text{noise and replicas at subband } l_{\min} \\ \vdots \\ \text{noise and replicas at subband } l_{\max} \end{bmatrix}. \tag{18}$$

We assume that noise plus replica interference is independent in each subband, and the covariance matrix of $\mathbf{V}'_u$ is

$$\mathbf{R}_u = \mathbb{E}\left[\mathbf{V}'_u\mathbf{V}'^H_u\right]$$
$$= \mathrm{diag}\,(\text{noise and replica interference power at subband } l_{\min}, \ldots, \text{noise and replica interference power at subband } l_{\max})\,. \tag{19}$$

The capacity of user u with the interference covariance matrix $\mathbf{R}_u$ is computed as

$$c_u = \log_2 \det\left(\mathbf{I}_{M_R} + \frac{\rho}{N_T}\mathbf{G}\mathbf{H}_u\mathbf{H}_u^H\mathbf{G}^H\mathbf{R}_u^{-1}\right). \tag{20}$$

Then, the sum capacity of the system is

$$\mathcal{R} = \sum_{u\in\mathcal{S}} c_u, \tag{21}$$

where $\mathcal{S}$ is the set of the scheduled users among the entire user set $\mathcal{U}$, i.e., $\mathcal{S} \subset \mathcal{U}$.

4 Replica interference avoidance strategy

Assuming no co-existing systems, the frequency-domain analysis in Section 3.2 have revealed that replica interference can be completely avoided if the beam pattern switching rate of the BSA receiver is an integer multiple of the product of the OFDM sampling rate and the number of receiving beam patterns. However, this does not hold

with co-existing systems. As shown in Fig. 4, oversampling rate Ω decides the spacing between adjacent replicas. Any possible overlaps of replicas from different co-existing systems result in performance degradation. This performance degradation depends on the choice of beam pattern switching rate $f_{\mathrm{SW}} = \Omega M_{\mathrm{R}} f_{\mathrm{S}}$. In this section, we consider three possible co-existing and cooperating scenarios in which replica interference degrades the system performance and propose the best-suit replica interference avoidance (RINA) strategy for each.

4.1 Maximum-capability RINA

In some co-existing cases, the system does not have any information regarding the co-existing status such as the number of neighboring systems and their distributions in the frequency bands. This situation occurs when the co-existing systems adopt different radio access technologies or no cooperating protocols are available. When there is no cooperating information from the co-existing systems, the best strategy for a single-RF MIMO-OFDM receiver with a BSA is to increase the beam pattern switching rate of the BSA to its maximum, which is referred to as maximum-capability RINA (MAX-RINA). The MAX-RINA strategy maximizes the spacing between replicas in the frequency domain, reducing the probability that the replicas of different systems overlap.

Figure 5 shows an example of MAX-RINA in which there exist three co-existing systems. Suppose that the existence of neighboring systems is completely unknown to system A. Based on the frequency-domain analysis in the previous section, the amount of replica interference that system A experiences depends on oversampling factor Ω. In the example, system A avoids replica interference from unknown system B for $\Omega \geq 2$ and avoids replica interference from unknown system C for $\Omega \geq 3$. Thus, using the maximum beam pattern switching rate is beneficial to avoid any potential replica interference from unknown neighboring systems. The major drawback of this approach is that it always enforces the use of the maximum switching rate capability of the BSA regardless of co-existing status. The overuse of the beam pattern switching capability results in high power consumption, which could be a significant burden to user devices.

4.2 Static RINA

We consider a limited cooperating case in which the system has partial knowledge of other co-existing systems. It is assumed that the system knows the number of co-existing systems that induce replica interference and degrade the system performance of each other. The simple solution in this case is that the co-existing systems use exclusive radio resources, i.e., subcarriers. The entire set of subcarriers is partitioned into multiple subgroups; each co-existing system uses only one of the subgroups not used by others. This restriction prevents any system from inducing replicas in subcarriers that are used by other co-existing systems. Because the partitioning and subgroup assignments need to be updated only when the co-existing status changes, this strategy is referred to as static RINA (S-RINA).

Figure 6 shows an example of S-RINA in which there exist three co-existing systems operated by the same network operator and they have nine subcarriers each. S-RINA partitions the available subcarriers into three subgroups. In the example, system A, system B, and system C use only subcarriers 1–3, subcarriers 4–6, and subcarriers 7–9, respectively. The primary advantage of this approach is that replica interference between co-existing systems is completely avoided using a minimal amount of cooperating information. The primary drawback is a reduction in the number of available subcarriers. Thus, S-RINA is well suit to interference-limited or low cell-loading environments.

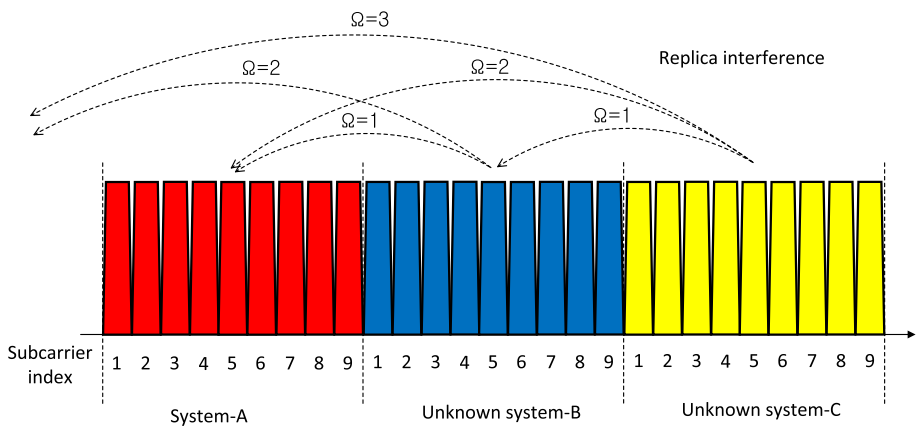

Fig. 5 Example of maximum-capability RINA with three co-existing systems and nine subcarriers

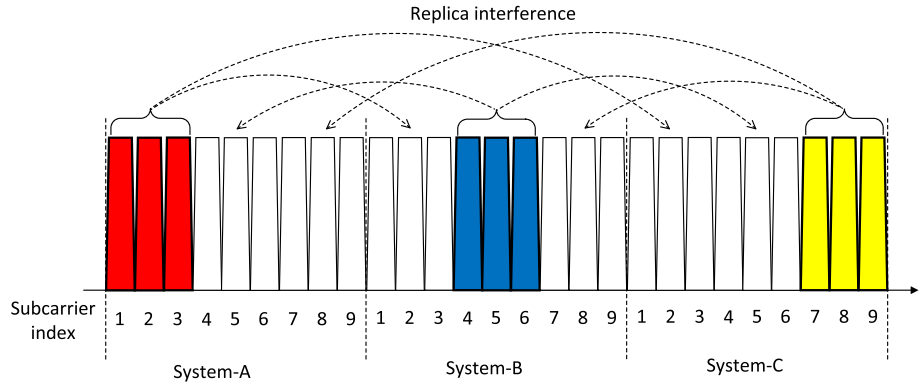

Fig. 6 Example of static RINA with three co-existing systems and nine subcarriers

4.3 Dynamic RINA

We consider a more aggressive cooperating case in which the system has full knowledge of all other co-existing systems. Full knowledge implies that the system knows not only the exact distribution of the co-existing systems in the frequency domain but also their scheduling information, including which subcarriers are currently selected for transmissions. This cooperating information can be exchanged through the backhaul. In recent advanced wireless systems, the backhaul is typically implemented with optical fibers. Hence, the impacts of latency and backhaul capacity are assumed minimal [33, 34]. Based on the cooperating information, the system can determine how each subcarrier is influenced by replica interference. Some subcarriers may be corrupted by the replicas of multiple co-existing systems. Only users with the high beam pattern switching capability can avoid the replica interference if they are allocated those subcarriers. On the contrary, some subcarriers may be corrupted by replicas of a small number of co-existing systems. Hence, most of the users (even those with low beam pattern switching capability) can avoid replica interference. Based on the observations above, the key principle of the proposed dynamic RINA (D-RINA) strategy is that the users are allocated subcarriers such that they can completely avoid replica interference using their own beam pattern switching capabilities. The proposed D-RINA algorithm is listed in Algorithm 1.

Algorithm 1 Dynamic RINA Algorithm

input Adjacent bands information $\mathcal{B} = \{1, 2, \ldots, N_{\mathrm{B}}\}$ and their subcarrier usage information Ψ_b ($b \in \mathcal{B}$).
Initialize $\mathcal{U} = \{1, 2, \ldots, N_{\mathrm{U}}\}$, $\Phi = \{1, 2, \ldots, N_{\mathrm{S}}\}$, $\mathcal{S} = \emptyset$, $\Psi = \emptyset$, and $\mathcal{W} = \emptyset$.
for all $k \in \Phi$ **do**
  Set $\bar{\mathcal{B}}_k = \{b | k \in \Psi_b\}$.
  Set $\Theta = \left\{\Omega | \mathrm{mod}\,(b_0, \Omega) \neq \mathrm{mod}\,(b, \Omega)\,,\ \mathrm{for} b \in \bar{\mathcal{B}}_k\right\}$.
  Compute $\bar{\Omega}_k = \min_{\Omega \in \Theta} \Omega$.
end for
repeat
  Compute $u^\star = \arg\max_{u \in \mathcal{U}} \Omega_u$.
  Set $\Delta = \left\{k \in \Phi | \bar{\Omega}_k \leq \Omega_{u^\star}\right\}$.
  Compute $k^\star = \arg\max_{k \in \Delta} \bar{\Omega}_k$.
  Update $\mathcal{U} \leftarrow \mathcal{U} \backslash u^\star$, $\Phi \leftarrow \Phi \backslash k^\star$, $\mathcal{S} \leftarrow \mathcal{S} \cup u^\star$, $\Psi \leftarrow \Psi \cup k^\star$, and $\mathcal{W} \leftarrow \mathcal{W} \cup \bar{\Omega}_{k^\star}$.
until $\mathcal{U} = \emptyset$ or $\Phi = \emptyset$.
return Selected user set $\mathcal{S}$, subcarrier set Ψ, and beam pattern switching rate set $\mathcal{W}$

A detailed description of the proposed D-RINA algorithm follows. The algorithm consists of two phases. In the first phase, the algorithm checks all subcarriers in Φ for the possible existence of replicas. Then, for each subcarrier k, the minimum required beam pattern switching rate $\bar{\Omega}_k$ required to avoid replicas on that subcarrier is determined. In the second phase, users are allocated subcarriers. The allocation starts with the user with the highest beam pattern switching capability Ω_u. Among the candidate subcarriers in which the user can avoid replica interference Δ, the user is allocated one that requires the maximum beam pattern switching rate. The determined user $u^\star$, subcarrier $k^\star$, and corresponding beam pattern switching rate $\bar{\Omega}_{k^\star}$ are added to the selected user set $\mathcal{S}$, Ψ, and $\mathcal{W}$, respectively. This process is repeated until all users or all subcarriers has been allocated.

Figure 7 presents an example of the proposed D-RINA algorithm, where there exist three co-existing systems operated by the same network operators and there are nine subcarriers in each system. Suppose that the reference system is on carrier A. Subcarrier 5 and 9 are used by carrier C; thus, it should be allocated to a user with the beam pattern switching capability greater than or equal to three ($\Omega_u \geq 3$). Since subcarrier 2 and 7 are used by carrier B, it should only be allocated to a user with a

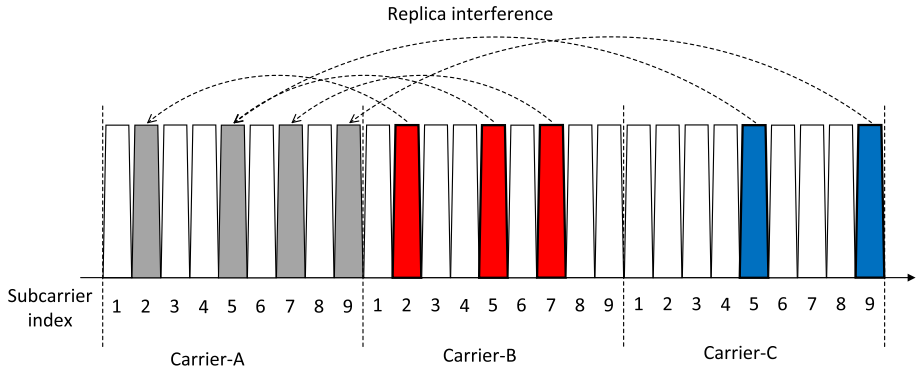

Fig. 7 Example of dynamic RINA with three co-existing systems and nine subcarriers

beam pattern switching capability greater than or equal to two ($\Omega_u \geq 2$). Finally, the remaining subcarriers are free from replica interference, so they can be allocated to any remaining users.

5 Overall network operations

We propose overall network operation principles to implement the D-RINA algorithm. A commercial LTE system [9] is considered in this study; however, principles are not limited to this case. Figure 8 presents the operating procedures in a timing diagram. After the users initially camp on their associated cells, the users need to report their basic device capabilities to their serving BS, which include the number of receiving beam patterns, M_{R}, and the maximum beam pattern switching capability, Ω. Based on periodic channel reports from the users, the BS determines the scheduling of the users and subcarriers; this scheduling information is then broadcasted to users. Note that, unlike that of the conventional systems, this scheduling information includes the appropriate beam pattern switching rate information for each scheduled user in the proposed D-RINA algorithm. This results in a small increase in downlink signaling overhead. Upon reception of the scheduling information, the scheduled users receive their desired signals at the indicated subcarriers with the indicated beam pattern switching rates. In addition, a part of the scheduling information, i.e., the set of scheduled subcarriers, is exchanged between other co-existing systems as cooperating information through the backhaul.

6 Simulation results

In this section, we compare the performances of different RINA strategies. The number of transmitting beam patterns is set to $N_{\mathrm{T}} = 4$. The number of receiving beam patterns is set to $M_{\mathrm{R}} = 4$. Rayleigh flat fading is considered for beamspace-domain MIMO channels. The

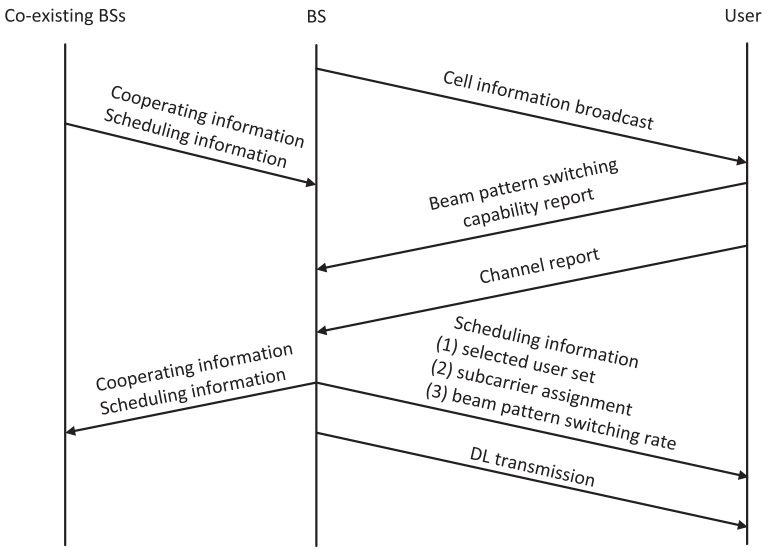

Fig. 8 Overall network operations of D-RINA

number of OFDM subcarrier is 128. The co-existing systems are assumed to be located in consecutive frequency bands. The cell loadings of the co-existing systems are set to 0.9. We consider different maximum beam pattern switching capabilities for different users. The maximum beam pattern switching capability of each user is randomly chosen from the integer set $[1, 2, \ldots, \Omega_{\max}]$ with equal probability. The sum rate is averaged over 1000 independent realizations of user channels.

Figure 9 shows how the average sum rate varies with SNR. S-RINA shows the worst performance in the low SNR region because the number of available subcarriers is strictly limited to avoid replica interference. In the high SNR region, the performance is limited by replica interference, and S-RINA outperforms the conventional BSA. MAX-RINA always enforces all users to enable maximum beam pattern switching capabilities, which increases the probability of avoiding replica interference. At the cost of overused processing power, MAX-RINA mitigates replica interference and outperforms S-RINA and conventional BSA. Finally, D-RINA outperforms all other schemes. D-RINA assigns subcarriers to users based on the users' beam pattern switching capabilities. This minimizes the chance of users being matched with subcarriers that require higher beam pattern switching capability than what the users have.

Figure 10 shows how the average sum rate varies with the number of users, i.e., cell loading. In general, the average sum rate increases with the number of users. With a small number of users, S-RINA provides the best performance. This is because replica interference is completely avoided and there are enough available subcarriers. However, as the number of users increases, the performance of S-RINA quickly saturates because of the shortage of available subcarriers. D-RINA and MAX-RINA outperform S-RINA as the number of users increases. Both schemes aim to use more subcarriers as the number of users increases. While the performance of MAX-RINA eventually saturates at $N_{\mathrm{U}} \geq 140$, that of D-RINA continues to increase even after $N_{\mathrm{U}} \geq 200$. This is because D-RINA efficiently exploits multi-user diversity for matching different beam pattern switching capabilities of users with subcarriers with replica interference.

Figure 11 shows how the number of co-existing systems degrades the system performance. As the number of co-existing systems increases, the available portion of subcarriers decreases accordingly, and the average sum rate of S-RINA decreases significantly. The average sum rates of MAX-RINA and D-RINA decrease at a much slower rate than that of S-RINA. In D-RINA, the performance degradation is minimal especially when there is a small number of co-existing systems. For example, the average sum rate decrease is approximately 0 % at $N_{\mathrm{B}} = 1$, and only 15.4 % at $N_{\mathrm{B}} = 2$, which is several-fold better than other schemes.

Figure 12 compares the average sum rate performances of different RINA strategies with respect to the maximum beam pattern switching rate of the BSA. In S-RINA and conventional BSA, users have only a basic beam pattern switching rate of $\Omega_u = 1$, and thus, the average sum rates are constant in all cases. As the maximum beam pattern switching rate increases,

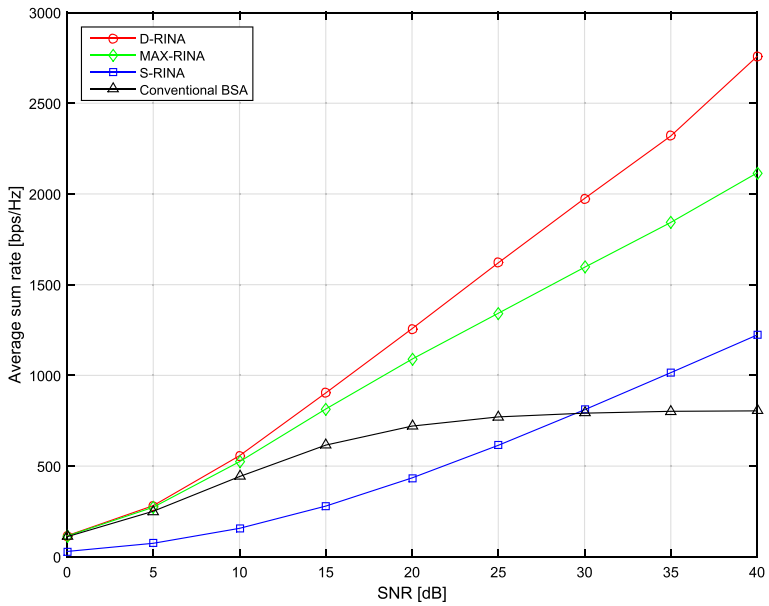

Fig. 9 Average sum rate versus SNR, where $N_{\mathrm{U}} = 200$, $\Omega_{\max} = 4$, and $N_{\mathrm{B}} = 3$

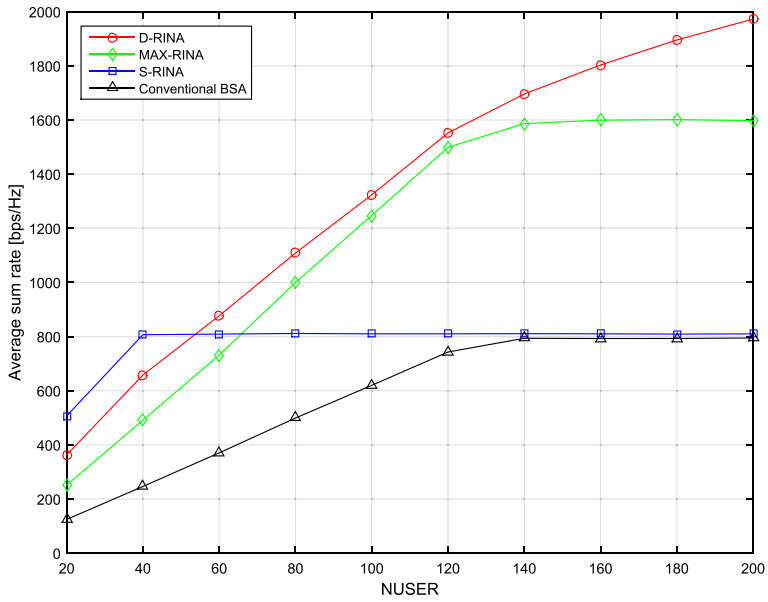

Fig. 10 Average sum rate versus number of users, where $\rho = 30$ dB, $\Omega_{\max} = 4$, and $N_B = 2$

the number of users with higher beam pattern switching capabilities increases. The average sum rate in D-RINA and MAX-RINA increases accordingly because they have a higher chance to avoid replica interference. Compared to MAX-RINA, D-RINA provides a much faster increasing rate, which confirms that D-RINA maximizes the benefits of users' beam pattern switching capabilities.

7 Conclusions

In this paper, we propose a single-RF MIMO-OFDM system with a BSA. We have solved the replica interference problem of a MIMO receiver with a BSA, which has, until now, been the primary impediment to practical implementations. We have presented two important findings. (i) Without any co-existing systems, replica interference in the system can be completely avoided if

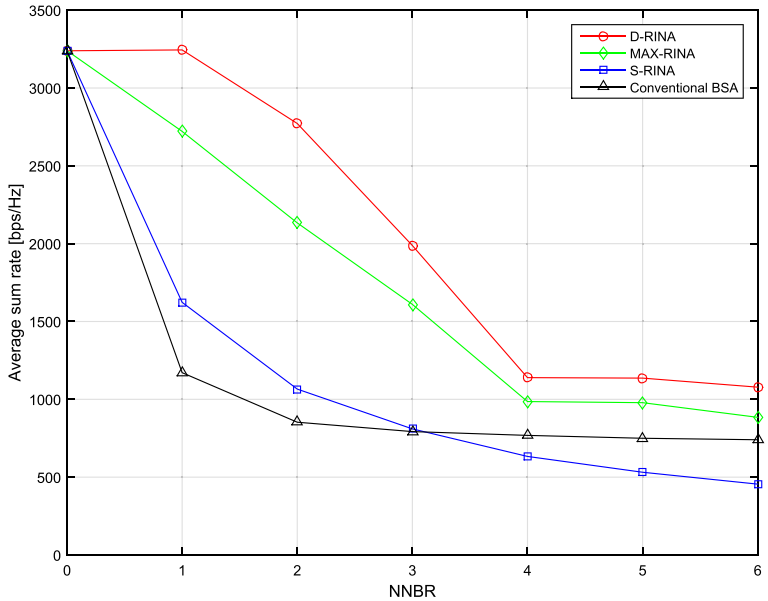

Fig. 11 Average sum rate versus number of co-existing systems, where $\rho = 30$ dB, $N_U = 200$, and $\Omega_{\max} = 4$

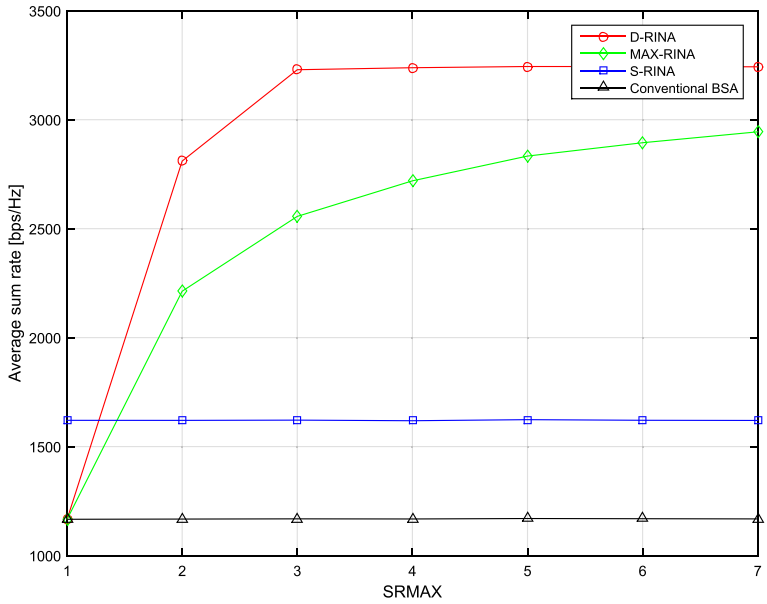

Fig. 12 Average sum rate versus maximum beam pattern switching rate, where $\rho = 30$ dB, $N_U = 200$, and $N_B = 1$

the beam pattern switching rate of a user is an integer multiple of the product of the OFDM sampling rate and the number of receiving beam patterns. (ii) With co-existing systems, replica interference in the system cannot always be avoided and the criterion as to whether each user experiences replica interference depends on the co-existing status and users' beam switching capabilities. We have considered three practical co-existence scenarios that are commonly encountered in commercial cellular systems. Three different RINA strategies are proposed for the scenarios. In addition, detailed network operation principles that adopt the proposed RINA algorithm have been described within the framework of commercial LTE systems. Future research directions will include channel estimation mechanisms, the extension to a multi-path channel model, and a more sophisticated investigation of beam switching patterns.

Competing interests
The authors declare that they have no competing interests.

Acknowledgements
This research was supported by Basic Science Research Program through the National Research Foundation of Korea (NRF) funded by the Ministry of Education (No. NRF-2015R1D1A1A01057100). This work was supported by Institute for Information & Communications Technology Promotion (IITP) grant funded by the Korea government (MSIP) (No. R0101-15-244, Development of 5G Mobile Communication Technologies for Hyper-Connected Smart Services).

Author details
[1]Department of Electronic Engineering, Gachon University, 461-701 Seongnam, Korea. [2]Communications and Internet Research Lab., ETRI, 305-700 Daejeon, Korea.

Received: 5 June 2015 Accepted: 26 January 2016

References

1. A Goldsmith, SA Jafar, N Jindal, S Vishwanath, Capacity limits of MIMO channels. IEEE J. Sel. Areas Commun. **21**(5), 684–702 (2003)
2. G Caire, S Shamai, On the achievable throughput of a multiantenna Gaussian broadcast channel. IEEE Trans. Inf. Theory. **49**(7), 1691–1706 (2003)
3. P Viswanath, D Tse, Sum capacity of the vector Gaussian broadcast channel and uplink-downlink duality. IEEE Trans. Inf. Theory. **49**(8), 1912–1921 (2003)
4. N Jindal, A Goldsmith, Dirty-paper coding versus TDMA for MIMO broadcast channels. IEEE Trans. Inf. Theory. **51**(5), 1783–1794 (2005)
5. I Sohn, JG Andrews, KB Lee, MIMO broadcast channels with spatial heterogeneity. IEEE Trans. Wirel. Commun. **9**(8), 2449–2454 (2010)
6. I Sohn, JG Andrews, Approaching large-system limits faster in multiuser MIMO with adaptive channel feedback adjustments. IEEE Commun. Lett. **14**, 1125–1127 (2010)
7. BA Bjerke, LTE-advanced and the evolution of LTE deployments. IEEE Wirel. Commun. **18**(5), 4–5 (2011)
8. Nokia Networks, LTE Release 12 and Beyond, 1–15 (2015). http://www.nsn.com
9. H Holma, A Toskala, *LTE for UMTS: Evolution to LTE-Advanced, 2nd Edition*. (Wiley, 111 River Street Hoboken, NJ 07030-5774, 2011)
10. TA Levanen, J Pirskanen, T Koskela, J Talvitie, M Valkama, Radio interface evolution towards 5G and enhanced local area communications. IEEE Access. **2**, 1005–1029 (2014)
11. E Perahia, R Stacey, *Next Generation Wireless LANs: 802.11n and 802.11ac*, 2nd ed. (Cambridge Univ. Press, New York, NY, USA, 2013)
12. Z Pi, F Khan, An introduction to millimeter-wave mobile broadband systems. IEEE Commun. Mag. **49**(6), 101–107 (2011)
13. TS Rappaport, S Sun, R Mayzus, H Zhao, Y Azar, K Wang, GN Wong, JK Schulz, M Samimi, F Gutierrez, Millimeter wave mobile communications for 5G cellular: it will work! IEEE Access. **1**, 335–349 (2013)
14. J Qiao, X Shen, JW Mark, Y He, MAC-Layer concurrent beamforming protocol for indoor millimeter-wave networks. IEEE Trans. Veh. Technol. **64**(1), 327–338 (2015)

15. B Li, Z Zhou, W Zou, X Sun, G Du, On the efficient beamforming training for 60 GHz wireless personal area networks. IEEE Trans. Wirel. Commun. **12**(2), 504–515 (2013)
16. Y Kim, H Ji, H Lee, J Lee, BL Ng, J Zhang, Evolution beyond LTE-advanced with full dimension MIMO. IEEE Int. Conf. Commun. Workshops (ICC), Budapest, 9–13 (2013)
17. YH Nam, BL Ng, K Sayana, Y Li, J Zhang, Y Kim, J Lee, Full-dimension MIMO (FD-MIMO) for next generation cellular technology. IEEE Commun. Mag. **51**(6), 172–179 (2013)
18. A Sayeed, N Behdad, Continuous aperture phased MIMO: basic theory and applications. IEEE Int. Conf. Communication, Control, and Computing Allerton, IL, USA, 1196–1203 (Sept. 29–Oct. 1 2010)
19. A Sayeed, Deconstructing multiantenna fading channels. IEEE Trans. Signal Process. **50**, 2563–2579 (2002)
20. A Kalis, A Kanatas, C Papadias, A novel approach to MIMO transmission using a single RF front end. IEEE J. Sel. Areas Commun. **26**, 972–980 (2008)
21. M Wennstrom, T Svantesson, An antenna solution for MIMO channels: the switched parasitic antenna. IEEE Int. Symp. Personal, Indoor and Mobile Radio Communications San Diego, CA, USA. **1**, A-159–163 (Sep. 2001)
22. K Gyoda, T Ohira, Design of electronically steerable passive array radiator (ESPAR) antennas. IEEE Int. Symp. Antennas and Propagation Society Salt Lake City, UT, USA. **2**, 922–925 (July 16–21, 2000)
23. MA Sedaghat, RR Mueller, G Fischer, A novel single-RF transmitter for massive MIMO. 18th International ITG Workshop on Smart Antennas (WSA) Erlangen, 1–8 (12–13 Mar. 2014)
24. Z Jin, J-H Lim, T-Y Yun, Small-size and high-isolation MIMO antenna for WLAN. ETRI Journal. **34**(1), 114–117 (2012)
25. R Bains, R Muller, Using parasitic elements for implementing the rotating antenna for MIMO receivers. IEEE Trans. Wireless Commun. **7**(11), 4522–4533 (2008)
26. M Yoshida, K Sakaguchi, K Araki, Single front-end MIMO architecture with parasitic antenna elements. IEICE Trans. Commun. **E95-B**(3), 882–888 (2012)
27. D Gwak, I Sohn, SH Lee, Analysis of single-RF MIMO receiver with beam switching antenna. ETRI Journal. **3**, 647–656 (2015)
28. V Barousis, AG Kanatas, N Skentos, A Kalis, Pattern diveristy for single RF user terminals in multiuser environments. IEEE Commun. Lett. **14**(2), 151–153 (Feb. 2010)
29. V Barousis, AG Kanatas, A Kalis, J Perruisseau-Carrier, Reconfigurable parasitic antennas for compact mobile terminals in multiuser wireless systems. EURASIP J. Wirel. Commun. Netw, 30 (2012). doi:10.1186/1687–1499-2012-30, Published: 3 Feb. 2012
30. S Shelley, J Costantine, CG Christodoulou, DE Anagnostou, JC Lyke, FPGA-controlled switch-reconfigured antenna. IEEE Antennas Wireless Propag. Lett. **9**, 355–96358 (2010)
31. CG Christodoulou, Y Tawk, SA Lane, SR Erwin, Reconfigurable antennas for wireless and space applications. Proc. IEEE. **100**(7), 2250–2261 (2012)
32. VI Barousis, AG Kanatas, A Kalis, Beamspace-domain analysis of single-RF front-end MIMO systems. IEEE Trans. Veh. Technol. **60**(3), 1195–1199 (2011)
33. 3GPP TSG-RAN WG1, Orange Telefonica, Backhaul modelling for CoMP, R1-111174 (Feb. 2011)
34. 3GPP TSG-RAN WG3, TSG RAN WG3, Reply LS to R3-070527/R1-071242 on Backhaul (X2 interface) Delay, R3-070689 (Mar. 2007)